Theoretical modelling and experimental investigations of the diode-pumped thin-disk Yb : YAG laser

1999 Quantum Electron. 29 697

(http://iopscience.iop.org/1063-7818/29/8/A07)

Quantum Electronics **29** (8) 697 – 703 (1999)

PACS numbers: 42.55.Rz; 42.55.Sa; 42.55.Xi

Theoretical modelling and experimental investigations of the diode-pumped thin-disk Yb : YAG laser

K Contag, M Karszewski, C Stewen, A Giesen, H Hügel

Abstract. The fundamental principles of the operation of a solid-state laser are presented for the case when the active element is a thin disk. An analytical model of this laser is developed. The model is used to calculate the influence of the various parameters on the operational efficiency of the laser. A detailed model is also developed for calculations relating to a specific laser design and this model takes account of the geometry of the active medium, of the diode pump configuration, and of the operating conditions. Experiments yielded a cw output power up to 350 W and an optical pumping efficiency of ~ 50% (the corresponding values obtained in this single-mode regime were approximately 100 W and 440%). These results were obtained below 0 °C for eight passes of the pump radiation through the active medium. At room temperature and for 16 passes the same parameters were several tens of watts and an efficiency up to 58%. These experimental results were in good agreement with the predictions of the theoretical model.

1. Lasers for material processing

Good-quality output radiation beams are needed in many applications of high-power lasers. A state-of-the-art review of this topic shows that solid-state lasers are significantly inferior to CO_2 lasers. Efficient utilisation of high-power lasers in industry requires a high quality of the radiation beam, efficient pumping, concentration of the energy on the workpiece, realibility, a long service life, and a compact size. Lasers emitting at $\lambda \approx 1$ μm or at shorter wavelengths are of considerable interest because of the stronger absorption of the laser radiation with these wavelengths by a majority of the materials of technical importance, and also because the undesirable effect of the laser plasma on industrial processes is less at these wavelengths.

Flashlamp- and diode-pumped Nd : YAG lasers are becoming increasingly popular in industry. In many of these lasers the flashlamps are simply replaced with laser diodes. However, this procedure fails to utilise all the advantages of diode pumping (see, for example, Ref. [1]). For example, optimisation of diode pumping and of the technique of cooling the active element was reported [2]. This has made it possible to use also quasi-three-level active media [3]. Studies have also been made of weakening the thermal lens effect in slab lasers.

As regards the beam quality, however, the principal advantages provided by diode pumping of solid state media, that is high efficiency and high beam quality, have not yet been fully exploited. Fig. 1 shows the beam quality parameter M^2 (the factor by which the beam divergence exceeds the diffraction limit), as a function of the cw output power. In the case of CO_2 lasers this parameter is close to one, whereas diode-pumped solid state lasers offer a potential improvement of almost 2 orders of magnitude even at high power levels.

A high beam quality can be obtained by appropriate resonator design and a rigorous reduction of the thermal effects inside the active medium. This means that the thermal lensing effects have to be avoided or controlled in such a way that no detrimental effects will occur. One possibility is to orient the heat flux collinearly with the direction of laser propagation, i.e., $\nabla T \| \boldsymbol{k}$. Consequently, the active medium has to be short compared with its diameter. Examples of this approach are active-mirror lasers [6], disk amplifiers [7], or thin-disk lasers which are cooled on one or both sides. Another possibility is to allow the propagation of only the fundamental transverse mode, defined by the condition $(d/\lambda)A_n < 0.766$, where A_n is the numerical aperture of the beam.

Owing to the higher possible output power per module, the thin-disk laser approach was studied in cooperation

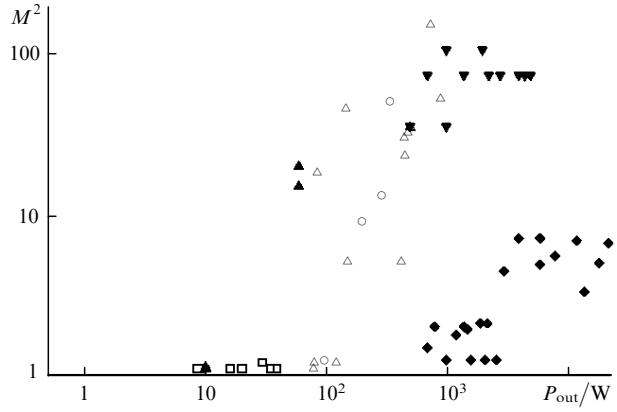

Figure 1. Dependences of the beam quality parameter M^2 on the output power P_{out}, obtained for various laboratory (open symbols) and commercially available (black symbols) lasers, including disk lasers (circles), fibre lasers (squares), solid-state lasers with diode (△, ▲) and flashlamp (▼) pumping, and also CO_2 lasers (◆).

K Contag, M Karszewski, C Stewen, A Giesen, H Hügel Institut für Strahlwerkzeuge (IFSW), Universität Stuttgart, Pfaffenwaldring 43, D-70569 Stuttgart, Germany;
tel.: +49 (711) 685 6858; fax: +49 (711) 685 6842;
email: stewen@ifsw.uni-stuttgart.de, karszewski@ifsw.uni-stuttgart.de, contag@ifsw.uni-stuttgart.de

Received 4 March 1999
Kvantovaya Elektronika **28** (2) 139 – 146 (1999)
Edited by L Dwivedi and A Tybulewicz

with IFSW, University of Stuttgart, and DLR, and this led to the development of the first thin-disk Yb : YAG laser in 1993 [8].

2. The concept of the thin-disk laser

A crystal disk with a thickness smaller than the diameter of the disk is mounted with one of its faces, which is high-reflectivity (HR) coated for both the laser and the pump wavelength, on a heat sink (Fig. 2). Therefore the excess heat is removed via this face. If we assume a large heat-transfer coefficient over the whole area, a temperature field will be established in the crystal with the isotherms essentially normal to the axis. The disk can be pumped by laser diodes either in a quasi-longitudinal scheme or radially. To increase the absorption of the pump radiation for a given thickness of the crystal, multiple passes of pump radiation through the disk can be used. This disk fits into the resonator as an end mirror (see Fig. 2) or as a folding mirror. The design is suitable for lasers in the power range of several watts to kilowatts, as demonstrated below. The power can be scaled by increasing the pumped diameter of the disk at constant pump power density and/or by using more than one disk. By employing the appropriate resonators and efficient cooling technologies, it is possible to achieve a high beam quality and a high efficiency simultaneously.

This design is particularly well suited for quasi-three-level systems such as Yb : YAG, because a low mean temperature of the crystal and a high pump power density are necessary for efficient operation. Therefore Yb : YAG was chosen as the preferred active medium. The properties of Yb : YAG have been discussed in detail elsewhere [9 – 11]. The thin-disk concept is also suitable for a variety of other laser materials. Operation with Nd : YAG, Nd : YVO_4, and Tm : YAG has been demonstrated [12 – 14].

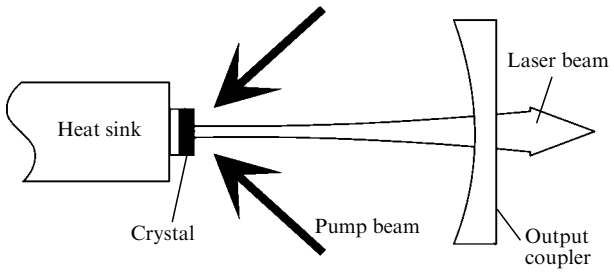

Figure 2. Optical scheme of the investigated thin-disk laser with quasi-longitudinal pumping of the crystal.

3. Modelling

An analytical and numerical model of the thin-disk laser, developed to describe the basic features of the quasi-three-level active medium Yb : YAG, is presented. The main results will be discussed by comparison with experimental data.

3.1 Analytical model

A quasi-three-level laser active medium, which is sometimes also termed a quasi-four-level medium, is characterised by a significant thermal population of the lower laser level. This means that the lasing properties change with temperature from those of a four-level system, where the lower laser level has no population at thermal equilibrium, to those of a three-level system, where the lower laser level is fully populated at thermal equilibrium. The main difference in the lasing properties between a true four-level system and a quasi-three-level system result from reabsorption losses at the laser wavelength, which increase the internal losses in the resonator and hence increase the lasing threshold.

The energy level system of Yb : YAG consists of the Stark-split $^2F_{7/2}$ ground state and the $^2F_{5/2}$ excited state [15]. Because of small energy splitting of each manifold, the relaxation times for energy levels within a manifold are assumed to be very small, of the order of picoseconds [16]. This justifies the use of a two-manifold model, where the cross sections $\sigma_{\mathrm{abs}}(\lambda, T)$ and $\sigma_{\mathrm{em}}(\lambda, T)$ for absorption and stimulated emission are related at any given wavelength λ and temperature T by a detailed balance relation [17]:

$$\sigma_{\mathrm{abs}}(\lambda, T) = f(\lambda, T)\sigma_{\mathrm{em}}(\lambda, T) \; . \tag{1}$$

The factor $f(\lambda, T)$, which relates the emission cross section to the absorption cross section, is given by

$$f(\lambda, T) = \frac{Z_{\mathrm{up}}(T)}{Z_{\mathrm{low}}(T)} \exp\left(\frac{hc/\lambda - E_{\mathrm{zpl}}}{k_{\mathrm{B}}T}\right) . \tag{2}$$

Here, $Z_{\mathrm{up}}(T)$ and $Z_{\mathrm{low}}(T)$ denote the partition functions of the upper and lower manifold, respectively; E_{zpl} is the energy of the zero-phonon line and is equal to the energy difference between the lowest level in the upper manifold and the lowest level in the lower manifold. The partition functions for each manifold m are given by

$$Z_m(T) = \sum_{i=0}^{n_m - 1} g_{mi} \exp\left(-\frac{E_{mi} - E_{m0}}{k_{\mathrm{B}}T}\right) , \tag{3}$$

where n_m is the number of energy levels E_{mi} within manifold m, and g_{mi} is the degeneracy of each energy level. Note that $\sigma_{\mathrm{abs}}(\lambda, T)$ and $\sigma_{\mathrm{em}}(\lambda, T)$ are not spectroscopic cross sections for transitions between specific energy levels, but describe transitions at arbitrary wavelengths between the two manifolds and depend on the population distribution within each manifold. The advantage of this description is that $\sigma_{\mathrm{abs}}(\lambda, T)$ is readily available from measured spectra without further calculation and that this model can easily be used in the calculation of laser tuning curves. At the same time, it is fully equivalent to a description where only transitions between specific energy levels are considered. In this case f would be given by the ratio $f_{\mathrm{low}}/f_{\mathrm{up}}$ where f_{low} is the fractional population of the level chosen in the lower manifold, and f_{up} is the fractional population of the level chosen in the upper manifold.

Expressions for the laser threshold and efficiency are derived below for a simple model of the laser, where the temperature inside the crystal is constant and the crystal is pumped homogeneously. The rate equations for the two-manifold system are then given by

$$\frac{\mathrm{d}n_{\mathrm{up}}}{\mathrm{d}t} = \frac{E_{\mathrm{p}}\lambda_{\mathrm{p}}}{hc} \frac{\eta_{\mathrm{abs}}}{N_{\mathrm{ion}}d} - \frac{n_{\mathrm{up}}}{\tau}$$

$$- M_{\mathrm{r}} \frac{E_{\mathrm{res}}\lambda_{\mathrm{las}}}{hc} [n_{\mathrm{up}}\sigma_{\mathrm{em}}(\lambda_{\mathrm{las}}) - n_{\mathrm{low}}\sigma_{\mathrm{abs}}(\lambda_{\mathrm{las}})] \; , \tag{4}$$

and

$$\frac{dE_{res}}{dt} = M_r E_{res} N_{ion}[n_{up}\sigma_{em}(\lambda_{las}) - n_{low}\sigma_{abs}(\lambda_{las})]\frac{cd}{2l_{res}}$$

$$-E_{res}\frac{c}{2l_{res}}[-\ln(1-T_{oc}) - \ln(1-L)] \ . \qquad (5)$$

Here n_{up} denotes the fraction of laser ions that are excited into the upper manifold, and n_{low} is the fraction of laser ions in the lower manifold; N_{ion} is the bulk density of laser ions; E_p is the power density of the pump radiation; hc/λ_p is the energy of a pump photon; η_{abs} is the absorption efficiency of the pump radiation; d is the crystal thickness; τ is the fluorescence lifetime of the upper manifold; E_{res} is the power density of the circulating laser radiation inside the resonator; M_r is the number of passes of the laser radiation through the crystal per resonator round trip; $\sigma_{em}(\lambda_{las})$ and $\sigma_{abs}(\lambda_{las})$ are the emission and absorption cross sections, respectively, at the transmission of the output coupler; l_{res} is the optical length of the resonator; L is the factor for the integrated losses per round trip.

Solving Eqn (5) for the steady-state conditions ($dE_{res}/dt = 0$) we obtain the required population of the upper manifold for laser operation n_{up}^{req}:

$$n_{up}^{req} = n_{up}^{trans}\frac{-\ln(1-T_{oc}) - \ln(1-L)}{M_r dN_{ion} f(\lambda_{las})\sigma_{em}(\lambda_{las})} + n_{up}^{trans} \ , \qquad (6)$$

where

$$n_{up}^{trans} = \frac{f(\lambda_{las})}{1+f(\lambda_{las})} \qquad (7)$$

defines the fraction of excited laser ions at which the laser material becomes transparent at the laser wavelength (here, T_{oc} is the transmission of the output coupler). For Yb : YAG at room temperature, n_{up}^{trans} is about 6.2%. Using expression (6) in Eqn (4) and solving for the output power density E_{out}, we obtain

$$E_{out} = T_{oc}E_{res} = \frac{T_{oc}}{-\ln(1-T_{oc}) - \ln(1-L)}$$

$$\times \eta_{abs}\eta_{st}(E_p - E_{th}) \ , \qquad (8)$$

where η_{st} denotes the Stokes efficiency $\eta_{st} = \lambda_p/\lambda_{las}$, and the threshold pump power density E_{th} is given by

$$E_{th} = \frac{hcdN_{ion}}{\lambda_p\eta_{abs}\tau}n_{up}^{req} = \frac{hc}{\lambda_p\eta_{abs}\tau}n_{up}^{trans}$$

$$\times\left[\frac{-\ln(1-T_{oc}) - \ln(1-L)}{M_r f(\lambda_{las})\sigma_{em}(\lambda_{las})} + dN_{ion}\right] . \qquad (9)$$

Eqns (8) and (9) clearly show the contradictory requirements concerning the crystal thickness of end-pumped quasi-three-level systems. On the one hand, the slope efficiency is proportional to the absorption efficiency of the pump radiation, which increases with crystal thickness. On the other hand, the laser threshold also increases with the crystal thickness, owing to reabsorption at the laser wavelength. The concept of a thin-disk laser is an elegant way to solve the dilemma. The use of multiple passes of the pump radiation through the crystal helps to reduce the crystal thickness while maintaining high absorption efficiency. The absorption efficiency is given by

$$\eta_{abs} = 1 - \exp(-M_p d\sigma_{abs}(\lambda_p)N_{ion}f_b) \ , \qquad (10)$$

where M_p is the number of pump beam passes through the crystal, and f_b is a bleaching factor which describes the bleaching of absorption due to inversion:

$$f_b = 1 - n_{up}^{req}\frac{f(\lambda_p) - 1}{f(\lambda_p)} \approx 1 - n_{up}^{req} \ . \qquad (11)$$

Since the absorption cross section $\sigma_{abs}(\lambda_p)$ as well as the emission cross section $\sigma_{em}(\lambda_{las})$ and the factor $f(\lambda_{las})$ depend on crystal temperature, the optimum crystal thickness and the optical efficiency that can be achieved are temperature-dependent. Fig. 3 shows the optical efficiency versus the pump power density at different crystal temperatures. The values were calculated for $M_p = 8$, and the crystal thickness was optimised for every data point. It clearly shows the detrimental effect of elevated crystal temperatures on efficiency, which means that effective removal of excess heat is essential for efficient operation. It also shows a considerable increase in the efficiency with the pump power density, owing to the relatively high threshold of the quasi-three-level material. This means that the brightness of the pump source is an important parameter in the laser design.

Fig. 4 shows the dependence of the optical efficiency on the crystal temperature for different numbers of pump beam passes. It clearly demonstrates the advantage of the thin-disk laser concept with multiple pump beam passes, especially at high crystal temperatures.

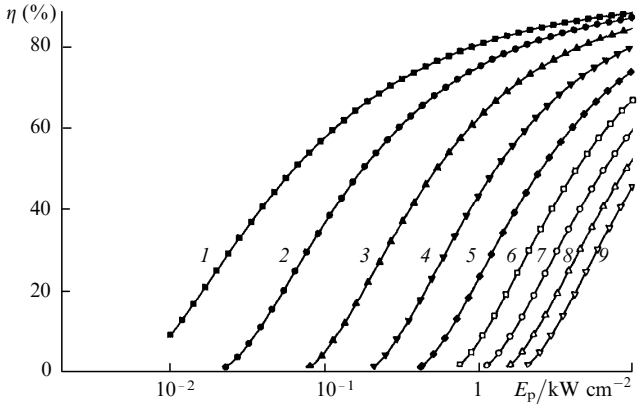

Figure 3. Dependences of the optical efficiency η on the pump power density E_p, obtained at the following effective crystal temperatures (K): *1*) 100; *2*) 150; *3*) 200; *4*) 250; *5*) 300; *6*) 350; *7*) 400; *8*) 450; *9*) 500.

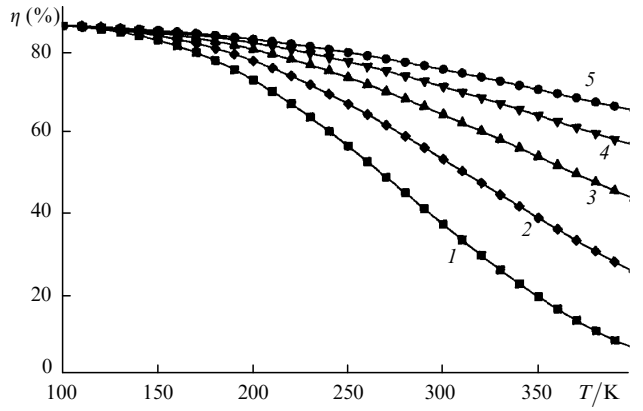

Figure 4. Dependences of the optical efficiency η on the crystal temperature T for various numbers of the pump-beam passes: *1*) 2; *2*) 4; *3*) 8; *4*) 16; *5*) 32.

3.2 Numerical model

The analytical model gives a general insight into the requirements concerning the pump power density, operational temperature, and crystal thickness for the design of a thin-disk laser. So far, however, the distribution of temperature inside the crystal has been neglected. A inhomogeneous temperature distribution leads to different pump absorption and different reabsorption of the laser radiation across the thickness of the crystal. Other analytical models for longitudinally pumped quasi-three-level systems that have been developed [18, 19, 20] do not account for this effect either.

In a real laser system, there is a discrete heat resistance at the boundary between laser crystal and cooling system, which must also be taken into account. As can be seen from Fig. 3, the optical efficiency depends strongly on the incident pump power density, which means that the distribution of pump power has an effect on the overall efficiency of the laser. For these reasons a numerical model [21] is used to calculate the optimum design parameters of the thin-disk laser used in our experiments.

The numerical model consists of three main steps. In the first step, the distribution of the absorbed pump radiation inside the crystal is calculated by Monte Carlo ray-tracing of the pump photons through the optical system. In the second step, the temperature distribution inside the crystal is calculated, according to the results of the ray-tracing calculation. In the third step of the model, the output power is calculated, taking into account the distributions of the pump radiation and of the temperature. These three steps are repeated iteratively until a steady state is reached. The three steps are described in more detail below.

3.2.1 Calculation of absorption

In calculation of the distribution of absorbed pump radiation within the crystal, a Monte Carlo is employed. The paths through the optical systems of a large number of photons are traced, with absorption being considered as a statistical process. Because of the high beam quality parameter of the pump diodes, geometric ray-tracing can be used. The starting position and the propagation direction of every single photon are chosen at random, according to the spatial dimensions of the pump source and the angular distribution of the pump radiation (i.e., the measured distribution of the pump radiation within the numerical aperture). The wavelength of the pump photons is determined randomly, according to an assumed Gaussian profile with the measured spectral width of the pump diodes. The path of every photon is traced through the system until it is lost at one of the optical components (i.e., it has missed the component), is absorbed within the crystal, or has exited the system after the designated number of passes through the crystal.

The transmission of the crystal along the photon path is calculated taking into account the photon wavelength, the temperature dependence of absorption, and the bleaching due to inversion. Whether or not the photon is absorbed is determined by comparison of a random number r, generated in the interval $(0, 1)$, with the calculated value T of the transmission. For $r > T$, the photon is absorbed and the distance l at which the photon is absorbed is $r = T(l)$. The crystal is divided into a mesh of finite elements with typically 60 elements in the radial direction, 20 elements in the axial direction, and 40 angular elements. The absorbed photons are counted in the corresponding element of the mesh. In order to minimise the computation time, parameters for the transmission of every element of the mesh are precomputed.

3.2.2 Calculation of temperature

As the distribution of the absorbed energy is usually symmetric around the axis of the crystal, the temperature is calculated for a rotational symmetry. Generation of heat is assumed to result from two mechanisms. The first is the Stokes effect of 8.7% between the energy of the pump and laser photon. The second source of heat is the absorption of the pump and laser radiation as well as fluorescence by the high-reflectivity coating of the crystal, and has been measured by calorimetry to amount to about 6% of the absorbed pump power. The heat load is calculated according to the distribution of the absorbed pump radiation and is applied to a two-dimensional mesh of elements. The temperature of every element of the mesh is adjusted by an iterative process until the heat flow to the neighbouring elements equals the generation of heat. A finite heat resistance between the crystal and the cooling medium is included in the calculations. The value of the heat resistance is determined from finite element calculations performed for a complete model of the crystal, including the reflective coating and the heat sink.

3.2.3 Calculation of the output power

In calculation of the output power, the symmetry of the pump radiation distribution is assumed to be rotational. The resonator is taken to be plane-parallel and infinitesimally short, so that the laser rate equations can be solved independently for every radial segment of the crystal. This approximation is valid for resonators with a high ratio of the pump beam diameter to the fundamental mode diameter, because in this case the laser mode profile adjusts to the gain profile of the crystal. Eqn (4) is solved for every element of the crystal in the steady state ($\mathrm{d}n_{\mathrm{up}}/\mathrm{d}t = 0$), with the temperature dependence of the parameters taken into account and the factor M_{r}, introduced as the number of laser beam passes through the crystal, replaced by the factor $M_{\mathrm{r}}(z)$, which describes the local intensity enhancement at the axial position z because of amplification:

$$M_{\mathrm{r}}(z) = \sum_{i=1}^{m/2} \big(\exp\{g[(2\mathrm{i} - 1)d - z]\} + \exp\{g[(2\mathrm{i} - 1)d + z]\}\big) \; . \tag{12}$$

In Eqn (12) m is the number of laser beam passes through the crystal and g is the gain coefficient at the radial position, averaged over crystal thickness. The internal power density E_{res} in the resonator is adjusted iteratively, until the gain and losses are balanced and Eqn (5) is satisfied with $\mathrm{d}E_{\mathrm{res}}/\mathrm{d}t = 0$.

3.2.4 Numerical results

Fig. 5 shows the calculated dependence of the optical efficiency (defined as the quotient of the laser output power and the incident pump power) on the crystal thickness for different numbers of pump beam passes. The calculations were performed for a crystal with 10% atomic dopant concentration, a cooling temperature of $T_{\mathrm{c}} = -30\ ^{\circ}\mathrm{C}$, and an incident pump power of 250 W, with a maximum pump power density of 6.5 kW cm^{-2}. The results show that the optical efficiency can be increased from 29% to 52% when 8 instead of 2 pump beam passes are used, and even to 62% with 16 passes. This advantage of multiple pump beam passes, which is even greater at higher cooling temperatures, led us to increase the number of pump beam passes from 8 to 16.

Another way to reduce the crystal thickness, and hence increase the optical efficiency, is to increase the dopant concentration. Fig. 6 shows the corresponding results of the numerical model. These calculations were made for 8 pump beam passes and the same parameters that were used for the calculations shown in Fig. 5. The material parameters were assumed to be independent of the dopant concentration. The results show that the optical efficiency increases only slightly when the optimum crystal thickness decreases. This is due to the fact that with the higher dopant concentration at reduced crystal thicknesses the total number of laser active ions in the pumped volume remains almost constant. This means that the reabsorption loss at the laser wavelength remains unchanged, in contrast to a reduction in the crystal thickness achieved by using multiple pump beam passes. In this case, the total number of the pumped laser active ions is reduced, which leads to a lower laser threshold and a higher slope efficiency.

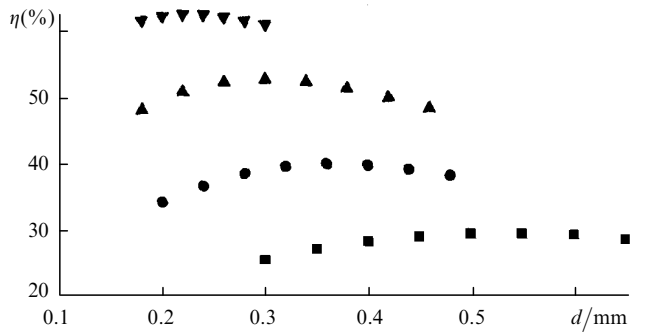

Figure 5. Numerically calculated dependences of the optical efficiency η on the crystal thickness d for various numbers of the pump-beam passes through the crystal: 2 (■), 4 (●), 8 (▲), 16 (▼).

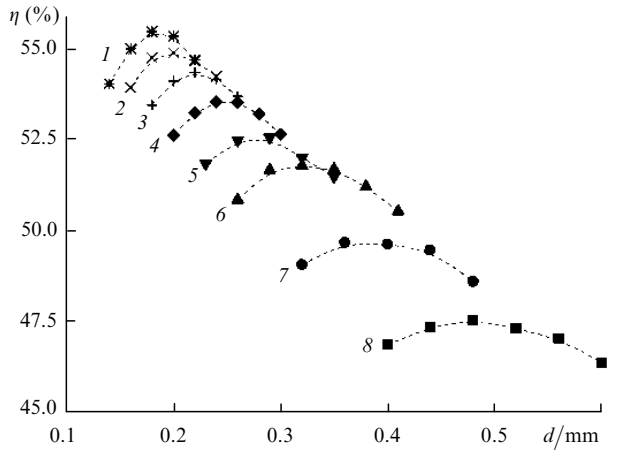

Figure 6. Numerically calculated dependences of the optical efficiency η on the crystal thickness d for various dopant concentrations (%): *1*) 6; *2*) 8; *3*) 10; *4*) 12; *5*) 14; *6*) 16; *7*) 18; *8*) 20.

4. Experimental results

The results obtained by using two different setups of the pump optics, allowing for 8 and 16 pump passes, respectively, are reported below. The scalability of the thin-disk concept and the dependence of the optical efficiency on the operational temperature and the beam quality are discussed in detail below.

4.1 Setup

Thin Yb:YAG disks with atomic dopant concentrations between 8% and 11% are used. A typical thickness is between 200 μm and 300 μm, according to the optimum values obtained by numerical calculations. A crystal is mounted with its back side on a cooled copper heat sink. The temperatures of the cooling fluid T_c was equal to room temperature, when water is used, and −70 °C, when alcohol is used. The crystal is HR-coated on its back side and Ar-coated on its front side for a pump wavelength of 941 nm and a laser wavelength of 1030 nm.

The first pumping scheme is the well-known setup [8] in which several mirrors are used to pass the pump radiation through the crystal (see Fig. 7). The disk is pumped with nearly constant and maximum pump power density at pumped diameters between 1.2 mm and 4.7 mm. The incident pump power densities are approximately 6.5 and 4.0 kW cm^{-2}, respectively.

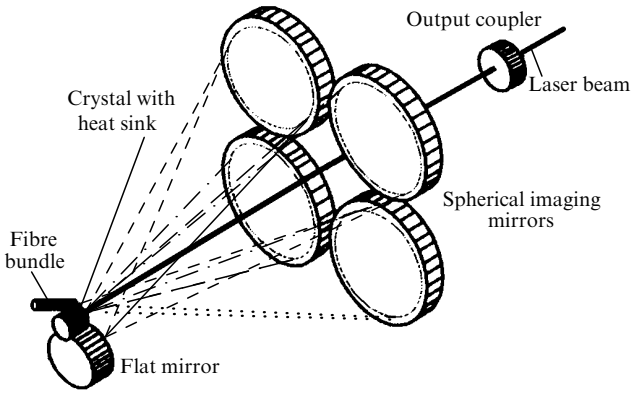

Figure 7. Schematic view of the investigated thin-disk laser with quasi-longitudinal pumping.

Owing to the 8 absorption passes this results in an effective pump power density of approximately 18 kW cm^{-2}, which is about 10 times above the threshold and should result in high efficiencies, according to the calculations presented in Fig. 5. Fibre-coupled InGaAs diode lasers (Opto Power Corp.) are used. The fibres are grouped into bundles of up to 19 fibres.

In a recently developed scheme, 16 absorption passes are achieved (Fig. 8). The pump radiation emerging from a single fibre-coupled diode laser is collimated by a spherical lens. A parabolic mirror with a crystal placed in its focal plane images the end of the fibre onto the crystal. The collimated beam uses only a 45° segment of a parabolic mirror. The

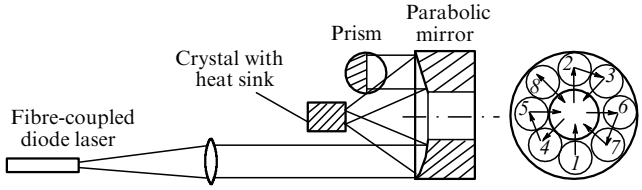

Figure 8. Schematic view of the second (new) pump design, which ensures 16 passes of the pump radiation through the crystal. The segments of the parabolic mirror are used as indicated by their numbers (shown on the right).

pump radiation emerging from the crystal after the first double pass through the crystal is collected by the adjacent segment of the mirror. The mirror collimates this beam. By use of a prism, the beam is reflected back onto the third segment of the mirror, imaged on the crystal, and so on, until the 8 segments of the parabolic mirror are used. This results in 8 absorption passes through the crystal. The remaining radiation emerging from the last segmentis reflected by a plane mirror so that the entire beam path is traversed in the opposite direction, giving a total of 16 passes.

4.2 Scalability of the output power

The output power of a thin-disk laser can be scaled by increasing the pumped diameter at a constant pump power density. In this way, several hundred watts of the output power can be obtained. Higher powers can be realised by using several disks in one resonator [14, 22].

Fig. 9 shows the results for 8 absorption passes and pumped diameters d_p of approximately 1.2 mm, 2.5 mm, 3.4 mm, and 4.7 mm, corresponding to approximately 60 W, 250 W, 500 W, and 700 W of the pump power, respectively. The resonator is formed by a coated crystal and a concave output coupler with a radius of curvature of 50 cm and with a transmission of 4%. The resonator is made as short as possible to achieve the highest efficiency. As expected, when the pumped diameter is increased the threshold pump power increases, but the threshold pump power density remains nearly constant. However, the slope efficiency η_{sl} decreases from 64% for $d_p = 1.2$ mm to 56% for $d_p = 4.7$ mm. This behaviour is confirmed by the numerical results. The calculations were made taking into account the shift of the wavelength of the pump diodes with the pump power and are included in Fig. 9. These calculations indicate an increasing contribution of three-dimensional heat conduction within the crystal with decreasing pumped diameter, which helps to lower the crystal temperature. Furthermore, the heat dissipating effect of the copper heat sink is reduced at larger pumped diameters and some material properties, e.g. the thermal conductivity, emissivity, and absorption cross section decrease with increasing temperature [23].

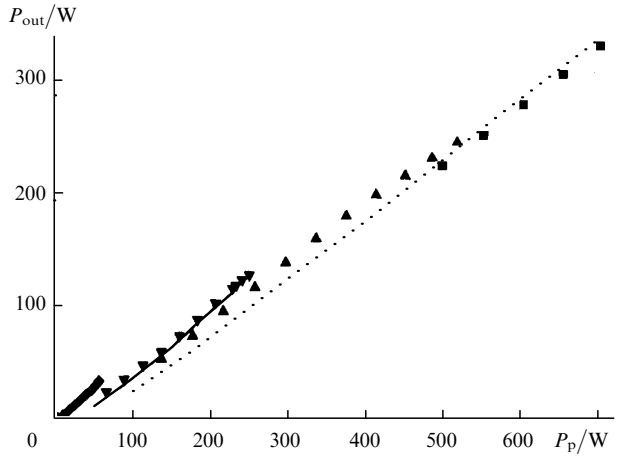

Figure 9. Scaling of the dependence of the output power P_{out} on the pump power P_p for eight passes of the pump radiation through the crystal, obtained for various diameters of the pumped region $d_p = 1.2$ mm (♦), 2.5 mm (▼), 3.4 mm (▲), and 4.7 mm (■), various temperatures of the cooling liquid $T_c = -28$ °C (♦, ▼), −67 °C (▲), and −52 °C (■), various values of $\eta_{sl} = 55\%$ (▲), 56% (■), 59% (▼), and 64% (♦), and comparison of the calculated (continuous curves for $d_p = 2.5$ mm, $T_c = -28$ °C, $\eta_{sl} = 59\%$, and dotted line for $d_p = 4.7$ mm, $T_c = -52$ °C, $\eta_{sl} = 56\%$) and experimental (black symbols) results.

4.3 Efficiency

The temperature dependence of the optical efficiency is shown in Fig. 10. With 8 passes of the pump radiation through the crystal and a pump power of 251 W ($d_p = 2.5$ mm) an optical efficiency of 52% is obtained at −28 °C. When a pump power of 58 W is used ($d_p = 1.2$ mm), the same efficiency is reached at 0 °C. This again indicates a higher mean temperature of the crystal for larger pumped diameters. The crystal used in these experiments had a thickness of 320 μm and an atomic dopant concentration of 11 %.

With the new pumping design, thinner crystals can be used. A crystal with a thickness of 240 μm and a dopant concentration of 10 at.% gives an optical efficiency of 58% at a temperature of the cooling fluid of 15 °C. As can be seen in Fig. 10, with 16 passes of the pump radiation at room temperature the same efficiency can be obtained as with 8 passes at −25 °C. This confirms that the mean temperature of the crystal is reduced by 40 °C in the case of the thinner crystal. An important consequence of the new pumping scheme is that it allows highly efficient room-remperature operation. The results of the numerical calculations are shown as straight lines in Fig. 10.

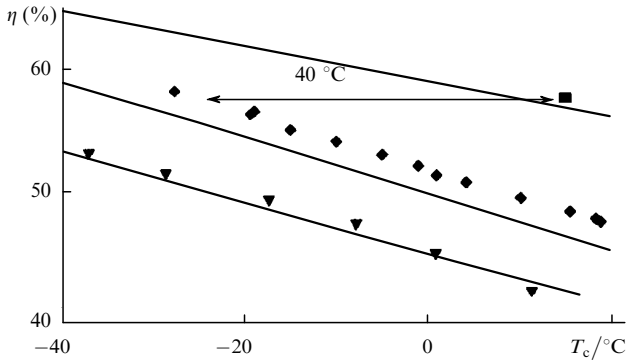

Figure 10. Experimental (black symbols) and calculated (continuous lines) dependences of the optical efficiency η on the temperature of the cooling liquid T_c for 8 (▼, ♦) and 16 (■) passes, through the crystal, of the pump radiation of 58 W (♦), 65 W (■), and 247 W (▼) power.

4.4 Beam quality

According to detailed investigations, the thermal lens of a thin-disk laser ranges from approximately 1 m to several meters. Using an appropriate resonator design, it is possible to achieve the best beam quality with M^2 as low as 1. In general, the resonator length and the radius of curvature of the output coupler should be chosen so that the desired M^2 value is obtained independently of the thermal lens. The aspherical contribution to the thermal lens is very low, so that TEM_{00}-mode operation can be highly efficient.

Fig. 11 shows the results obtained so far. With a pumped diameter of 1.2 mm and a pump power of 65 W, the M^2 values of between 8 and 1.0 were obtained at efficiencies greater than 50% (all the M^2 values were measured with a Coherent Modemaster meter). In these experiments, several resonator lengths between 10 cm and 50 cm, and output couplers with a radius of curvature of 0.5 m, 1.0 m, and 2.0 m, were used. The

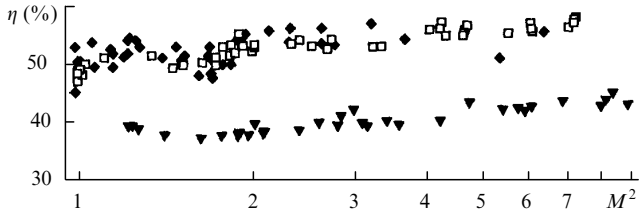

Figure 11. Dependences of the optical efficiency on the beam quality parameter M^2 for 8 (▼, ◆) and 16 (□) passes, $T_c = 15$ °C (□), −9 °C (▼), and −40 °C (◆), $P_p = 65$ W (□), 66 W (◆) and 247 W (▼), demonstrating that the optical efficiency (and, consequently, of the output power of investigated disk laser) is practically independent of the beam quality.

measured output power, and hence the efficiency, was nearly independent of the resonator, indicating very low diffraction losses and a very small aspherical contribution to the thermal lens of the thin-disks. Obviously the spherical contribution to the thermal lens can easily be compensated by use of an appropriate resonator design. With a typical electrical-to-optical ('plug') efficiency of the fibre-coupled diode laser of 35%, an electrical-to-optical efficiency of the thin-disk laser of more than 17% was achieved.

With a maximum pump power of 247 W, the dependence of the efficiency on the beam quality was also investigated (Fig. 11) [24]. The temperature of the cooling fluid was −9 °C, and there were 8 passes of the pump radiation through the crystal. Once again, the efficiency was nearly independent of the beam quality. Using a resonator with a length of 185 cm, an output coupler with a curvature of 2 m, and a transmission of 4%, a value of $M^2 = 1.22$ was obtained. The output power of 97 W corresponds to the 39% optical efficiency and more than the 13% plug efficiency, when the measured electrical efficiency of 34% of the fibre-coupled diode lasers is taken into account. With the shortest possible resonator used, without an emphasis on the beam quality a maximum output power of 110 W was achieved ($M^2 = 8.4$).

5. Summary

Both an analytical model and a numerical model of an Yb : YAG thin-disk laser have been presented. These were used to assess the main design parameters of the laser system. They demonstrate the advantage of the thin-disk laser concept in which multiple pump beam passes are used: a reduced crystal thickness leads to low temperatures inside the crystal, a low lasing threshold, and hence increases the optical efficiency of a quasi-three-level laser active medium. The scalability of the thin-disk laser concept was shown experimentally with cw output powers up to 350 W at an optical efficiency of 50%. Using 16 pump beam passes, an optical efficiency of 58% at room temperature was achieved. Experimental results show that, because of the weak thermal lens with the thin-disk laser concept, a high efficiency and a good beam quality can be attained nearly independently of the power level.

Acknowledgements. Parts of this work have been supported by the Bundesministerium für Bildung and Forschung under contracts 13N6364, 13N6465, and 13N7300. The assistance of S Böhm, S Erhard, R Greschner, J Häussermann, I Johannsen, T Rupp, C Schmitz, H Seyfried, and A Voss is gratefully acknowledged.

References

1. Brand T *BMBF Abschlussbericht* **13** (6358) (1995)
2. Schöne W, Knoke S, Schirmer S, Tünnermann A *OSA TOPS* **10** 292 – 295 (1997)
3. Bruesselbach H, Sumida D S, Reeder R, Byren R W *OSA TOPS* **10** 285 – 287 (1997)
4. Du K, Wu N, Xu J, Giesekus J, Loosen P, Poprawe R *Opt. Lett.* **23** 370 – 372 (1998)
5. Baker H J, Chesworth A, Millas D P, Hall D R *OSA TOPS* **19** 407 – 410 (1998)
6. Morris P J, Lüthy W, Weber H P *Opt. Commun.* **104** 97 – 101 (1993)
7. Koechner W *Solid State Laser Engineering* (Berlin: Springer, 1992)
8. Giesen A, Hügel H, Voss A, Wittig K, Brauch U, Opower H *Appl. Phys. B* **58** 365 – 372 (1994)
9. Fan T Y *IEEE J. Quantum Electron.* **29** 1457 – 1459 (1993)
10. Lacovara P, Choi H K, Wang C A, Aggarwal R L, Fan T Y *Opt. Lett.* **16** 1089 – 1091 (1991)
11. Bruesselbach H W, Sumida D S, Reeder R A, Byren R W *IEEE J. Sel. Top. Quantum Electron.* **3** 105 – 116 (1997)
12. Diening A, Dicks B-M, Heumann E, Huber G, Voss A, Karszewski M, Giesen A *International Conference on Lasers and Electro Optics (CLEO'98), San Francisco, 1998*, Paper CWF46
13. Koch R, Hollemann G, Clemens R, Voelckel H, Giesen A, Voss A, Karszewski M, Stewen C *International Conference on Lasers and Electro-Optics (CLEO'97), Baltimore, MD 1997* (OSA Technical Digest Series, Vol. 11) p. 480
14. Hügel H, Bohn W L *Proc. SPIE Int. Soc. Opt. Eng.* **3574** 15 – 28 (1998)
15. Bogomolova G A, Vylegzhanin D N, Kaminskii A A *Zh. Eksp. Teor. Fiz.* **69** 860 (1975) [*Sov. Phys.-JETP* **42** 440 – 446 (1975)]
16. Hall D W, Weber M J, Brundage R T *J. Appl. Phys.* **55** 2642 (1984)
17. McCumber D E *Phys. Rev. A* **134** 299 – 306 (1964)
18. Fan T Y, Byer R L *IEEE J. Quantum Electron.* **23** 605 – 612 (1987)
19. Risk W P *J. Opt. Soc. Am. B* **5** 1412 – 1423 (1988)
20. Taira T, Tulloch W M, Byer R L *Appl. Opt.* **36** 1867 – 1874 (1997)
21. Contag K, Brauch U, Erhard S, Giesen A, Johannsen I, Karszewski M, Stewen C, Voss A *Proc. SPIE Int. Soc. Opt. Eng.* **2986** 23 – 34 (1997)
22. Contag K, Brauch U, Giesen A, Johannsen I, Karszewski M, Schiegg U, Stewen C, Voss A *Proc. SPIE Int. Soc. Opt. Eng.* **2986** 2 – 9 (1997)
23. Sumida D S, Fan T Y *OSA TOPS* **20** 100 – 102 (1994)
24. Karszewski M, Brauch U, Contag K, Erhard S, Giesen A, Johannsen I, Stewen C, Voss A *OSA TOPS* **19** 296 – 299 (1998)